Crystal structure of poly(tetrafluoroethylene) homo- and copolymers in the high pressure phase

R. K. Eby
Institute of Polymer Science, The University of Akron, Akron, OH 44325-3909, USA

E. S. Clark
University of Tennessee, Knoxville, TN 37996, USA

B. L. Farmer
University of Virginia, Charlottesville, VA 22901, USA

G. J. Piermarini and S. Block
National Institute of Standards and Technology, Gaithersburg, MD 20899, USA
(Received 9 November 1989; revised 5 June 1990; accepted 2 July 1990)

X-ray diffraction measurements are reported for 27°C, pressures to 5.2 GPa and concentrations of CF_3 units to 0.049 CF_3/CF_2. These show both orthorhombic and monoclinic structures to exist under high hydrostatic pressure. It is proposed that shear stresses generated at elastic inhomogeneities in the sample lead to the monoclinic phase. Energy calculations are consistent with this concept. They also indicate that conformational and rotational disorders raise the entropy of the high pressure phase III. Perfluoromethyl branches increase the volume/CF_2 of phase III more than that of the low pressure phase I. At high CF_3 concentrations and pressures, both phases become metrically hexagonal. The volume of transition becomes zero at a concentration near 0.05 CF_3/CF_2 and no transition is observed to a pressure of 5.2 GPa. There appears to be a critical point near 27°C, a CF_3 concentration of 0.05 and a pressure of 3.5 to 5 GPa.

(Keywords: tetrafluoroethylene; hexafluoropropylene; copolymers; pressure; phase diagram; critical point; X-ray; defects; monoclinic; orthorhombic; energy calculations)

INTRODUCTION

The homopolymer, poly(tetrafluoroethylene) (PTFE), exhibits four crystal phases and the melt on a pressure–temperature phase diagram[1–5]. This diagram has been extended at one atmosphere to include the concentration of comonomer units of hexafluoropropylene[6]. The structures of the low pressure crystal phases, I, II and IV, have been studied extensively and are relatively well understood[7–13]. Above about 0.7 GPa at room temperature, the molecules untwist from the low pressure helical conformation to a planar zigzag conformation in phase III as indicated by spectroscopic data[14]. This phase and the transition to it have been investigated previously[15,16]. One study of the crystal structure using X-ray diffraction[17] has indicated a structure similar to that of monoclinic polyethylene[18], whereas another X-ray study[19] has indicated a structure similar to that of orthorhombic polyethylene[20]. It has been proposed[17,19] that a pressure cell with diamond anvils (as was used to observe the monoclinic phase[17]) must lead to a stress that is not purely hydrostatic. This article reports the results of an investigation of the structure of the high pressure phase by X-ray diffraction from a sample held under hydrostatic pressure in a diamond anvil cell. Experimental data are presented not only for the homopolymer but also for samples with a comonomer of hexafluoropropylene which has a strong influence on the structures, disorders and phase diagram at one atmosphere[6,13]. Energy calculations made with empirical pair potentials are used to help define the structures/disorders of the homopolymer. An extended phase diagram is presented.

EXPERIMENTAL METHODS

X-ray method

The experiments were carried out with the polymer samples contained in a diamond anvil high pressure cell. The diffraction measurements were made in the energy dispersive mode using unfiltered radiation from either a fixed anode of tungsten or a rotating anode of copper to yield a powder pattern in a manner described previously[21]. In order to enhance diffraction intensities, a larger sample volume than normal was required. A gasket containing a cylindrical sample chamber with a diameter of 0.3 mm and a height of 0.56 mm was used. To provide a hydrostatic pressure, the polymer sample, in the form of a rod 0.2 mm long and 0.36 mm in diameter, was encapsulated with a pressure transmitting liquid of a 4:1 volume mixture of methanol:ethanol[22]. Commonly used gasket materials, Inconel X750 and 301 stainless steel, did not provide the necessary thickness at 5 GPa to meet the sample-volume requirement for this study. Therefore, the material used was Vascomax 300

0032-3861/90/122227-11

which permits relatively large gasket thickness to be maintained in the 5 GPa pressure regime because of its higher yield strength. As a result, the sample is subject to hydrostatic pressure rather than the uniaxial stress that results when the gasket yields[19]. Observations with an optical microscope confirmed that when the cell was at pressure, the sample was not pinched by the surfaces of the top and bottom diamond anvils. Further, the sample either did not touch the side of the cylindrical chamber or touched it in only one place. A small ruby sphere, approximately 5 μm in diameter, was also placed in the sample chamber so that pressures could be measured by the fluorescence method[23]. The diffraction measurements were made at a two theta angle of 10° with exposure times ranging from 24 to 96 h, at pressures to 5.2 GPa, and a temperature of about 27°C. Background scattering was measured for the cell containing only the methanol:ethanol liquid. Scattering from the gasket was measured by offsetting the empty cell so that the beam impinged on the edge of the gasket.

Samples

Samples with CF_3 concentrations of 0, 0.008, 0.018, 0.034, 0.038 and 0.049 CF_3/CF_2 were used. These are samples 20, 14, 1, 15, 5 and 11, respectively, of reference 6. Samples 20, 14, 1 and 15 were used in reference 13. Sample 20 was used in reference 5. Samples 20, 1 and 11 are the first, second and sixth samples, respectively, in Figure 2 and sample 5 is in Figure 1 of reference 34. Note that the CF_3 concentrations in reference 34 were measured with an earlier method. All the samples except 15 were unoriented.

Computational modelling

Energy calculations were performed using either the Sybyl® molecular modelling software or a program and interatomic energy parameters that have been used to study the low pressure phases of PTFE[11,12]. Calculations with the latter were carried out using internally rigid molecular fragments containing 15 CF_2 units with bond lengths of 0.1534 nm and 0.134 nm for C–C and C–F lengths, respectively, and C–C–C and F–C–F bond angles of 117.3 and 109.0°, respectively. The translational advance was 0.131 nm/CF_2. The nine-stem array in *Figure 1* was used for calculations of the minimum energy structures. It allows direct comparison between orthorhombic and monoclinic energies, but has the disadvantage of slightly overemphasizing some of the molecular interactions in the orthorhombic structure. To eliminate this and to provide comparison with the energies of the helical structures[12], an array with 19 stems (*Figure 1*) of 45 CF_2 units each was next used. The interactions of the central 15 CF_2 units of the central molecule with the surrounding array were computed to atomic separations of 1.2 nm. One-thirtieth of this energy approximates the heat of vaporization of a CF_2 unit.

To simulate the effects of pressure on the monoclinic structure, various cell dimensions consistent with an appropriate area/stem were generated using 0.005 nm increments of the unit cell parameters, $a/2$ and b. The value of γ was adjusted to give the required area. Energies were then calculated (using the nine-stem model) for this set of cell dimensions. Typically about 75 sets of a, b and γ were examined for each area/stem. Care was taken to assure that the values of a, b and γ corresponding to the lowest energy were not at the limits of the ranges considered. The treatment of the orthorhombic structure was analogous except that γ was fixed at 90°. Increments of 0.01 nm were used for a, and b was adjusted to give the required area per stem. For the a and b values giving the lowest energy at each area/stem, the energy was minimized with respect to the setting angle of the stem, measured from the bc plane.

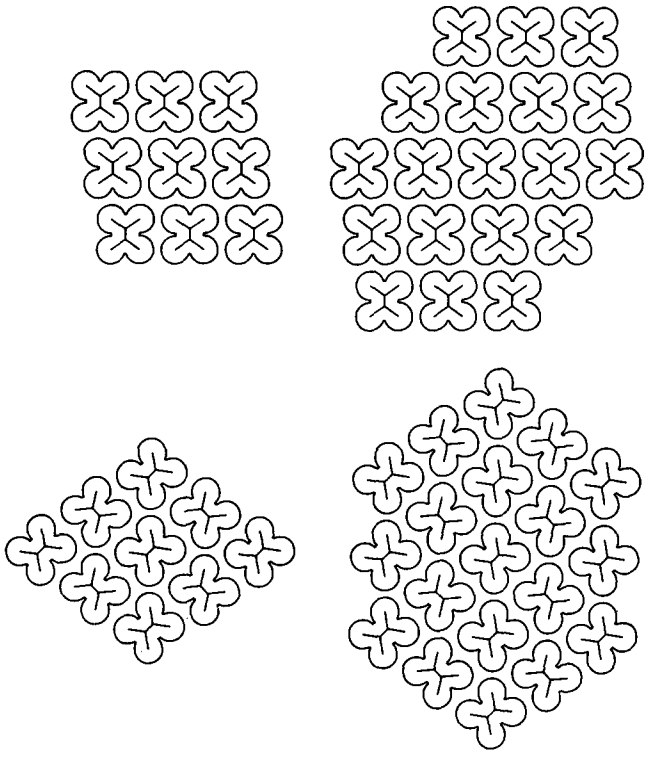

Figure 1 Schematic representation of the basal projections of the nine and 19 stem arrays of the monoclinic (top) and orthorhombic (bottom) structures

Energies were also determined for single stems having 15/7, 54/25, and 2/1 conformations placed at the central position of the low-energy nine-stem array and rotated in 6° increments[12]. For each low-energy orientation, the energy was minimized by placing the defect stem containing 15 CF_2 units at the desired setting angle in a 19-stem array and making small adjustments in the setting angle and translational position parallel to the stem axis (using increments of 1° and 0.025c, respectively). The dimensions of the whole array were then optimized (increments of 0.001 nm for a and b, and 1° for γ). Next, each of the six neighbouring stems was allowed to adjust its position to accommodate the defect (increments of 0.01a, 0.01b, 0.025c and 1°). Finally, the array dimensions were adjusted again. Because this process spreads the excess energy of the defect over the entire array, the energy of the defect was taken as the difference in energy between this minimized array and the perfect 19-stem array.

RESULTS AND DISCUSSION

Structures present

The difference between the lower pressure helical conformation with hexagonal packing and the higher pressure planar zigzag conformation with orthorhombic packing is readily evident in the corresponding powder patterns. *Figure 2* shows the diffracted intensity for PTFE

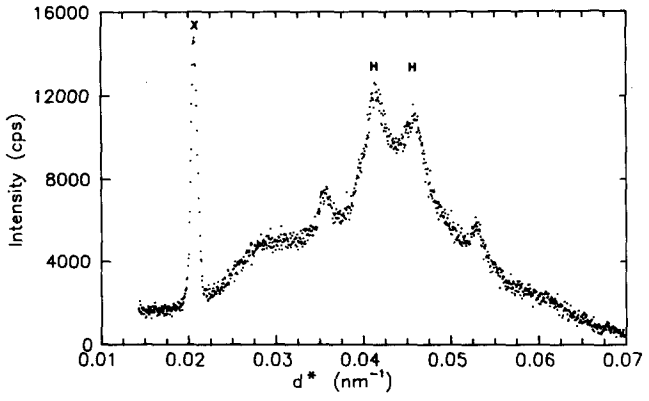

Figure 2 Powder diffractogram for PTFE homopolymer in phase II at 0.3 GPa. The inverse of the *d*-spacing is indicated by *d**. The marked peaks are discussed in the text

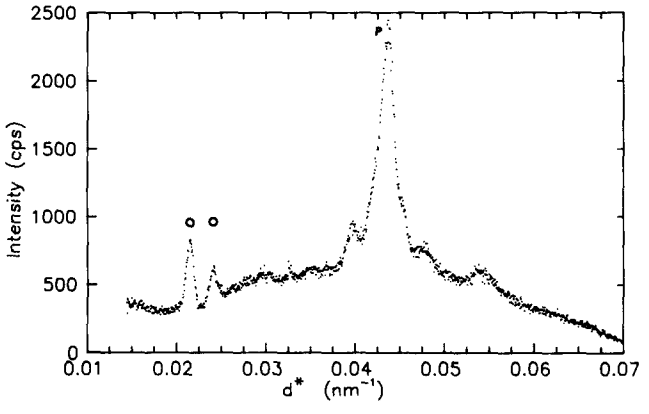

Figure 3 Powder diffractogram for PTFE homopolymer in phase III at 0.95 GPa. The inverse of the *d*-spacing is indicated by *d**. The marked peaks are discussed in the text

at a pressure of 0.3 GPa (phase II) as a function of d^*, the reciprocal of the *d*-spacing. *Figure 3* shows the same variables at 0.95 GPa (phase III). The lateral packing of the molecules can be inferred from the region of 0.02 to 0.03 nm^{-1}. A single peak, X, indexed (100), indicates the very nearly hexagonal packing of phase II in *Figure 2* (exactly hexagonal in phase I). A splitting of this peak in two, O, corresponding to the 110/200 pair, with an approximate ratio of 2:1 in intensity, indicates orthorhombic packing in *Figure 3*. The conformation of the molecules can be inferred from the region of about 0.04 to 0.05 nm^{-1}. The single peak, P, in *Figure 3*, indexed as (111), indicates a planar zigzag conformation. The splitting of this peak in *Figure 2* into two, H, indexed as (1 0 25)/(1 0 29), indicates that the conformation is 54/25[10] (in phase I these would be indexed as (107)/(108) for the 15/7 conformation).

A small amount of the monoclinic structure is also evident at pressures above about 2 GPa. *Figure 4* shows the diffracted intensity as a function d^* at a pressure of 3.9 GPa. The monoclinic phase is most readily apparent in this diffraction pattern. In the ranges of 0.02 to 0.03 nm^{-1} and 0.04 to 0.05 nm^{-1}, there are five additional peaks (marked) which cannot be indexed by the orthorhombic structure. The peak at approximately 0.048 nm^{-1} (denoted by *) is from the Vascomax gasket. The other four are from neither the gasket nor the ruby sphere but are consistent with the presence of a monoclinic structure. Since the pressure is hydrostatic, only the orthorhombic structure should be formed[19].

Formation of the monoclinic structure in polyethylene requires a shear deformation of the orthorhombic one[18,24]. In view of the similarity of the structures involved for PTFE[17,19] and polyethylene[18,20], it is reasonable to expect that a source of shearing might induce a phase change in PTFE also. One possible source is the presence of elastic inhomogeneities arising from either the micropores in the sample (which was processed by sintering) or the relatively large crystals[25]. These can produce large local shear and tensile stresses even though the sample is subject only to hydrostatic pressure[26–28]. This route of formation is also consistent with the variation from sample to sample in the amount of monoclinic material. Since the amount is usually small, its detection would be sensitive to the concentration and disposition of the inhomogeneities.

It is not certain why the monoclinic structure is not observed unambiguously below about 2 GPa. One possibility is that the shear stresses generated are not great enough below 2 GPa to produce a sufficient amount of the structure to be observed. Another is that the first monoclinic peak and the orthorhombic 110 peak move closer together at lower pressures as do the second monoclinic peak and the orthorhombic 200. This would preclude resolution of the smaller monoclinic peaks. The overlapping of the peaks would also influence the results of reference 17 unless only rather small amounts of the orthorhombic structure were present.

Orthorhombic homopolymer

The unit cell dimensions, *a* and *b*, are plotted as a function of pressure in *Figure 5*. To facilitate the comparison of phases II and III, the very nearly hexagonal lateral packing of the helices in phase II is reassigned in terms of a centred orthorhombic lattice with the *b*/*a* ratio equal to 0.577. The transition from phase II to phase III occurs between 0.67 and 0.7 GPa with a marked decrease in *a* and a much smaller increase in *b*. The data from reference 19 are also shown. Phase III was observed at a lower pressure in that work because the temperature of measurement was 78°C. The data reproduced here have been corrected slightly to 27°C using the expansion coefficient[16]. They represent reasonable extrapolations of the present data. The *c* dimension exhibits little change with pressure except for an increase of 0.0002 nm of the average value for phase III over that

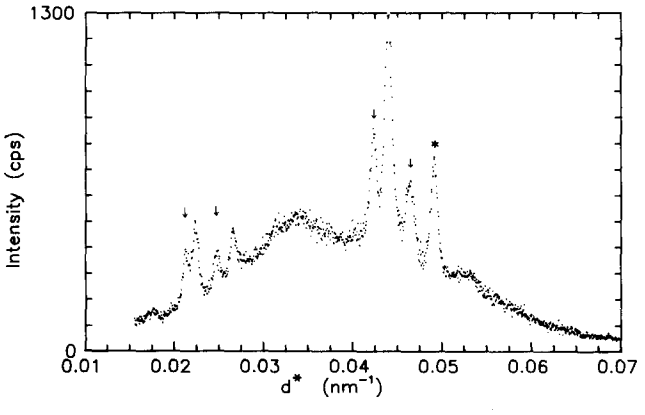

Figure 4 Powder diffractogram for PTFE homopolymer at 3.9 GPa. The inverse of the *d*-spacing is indicated by *d**. Arrows indicate peaks not attributable to the orthorhombic structure. The peak denoted by an asterisk is from the gasket

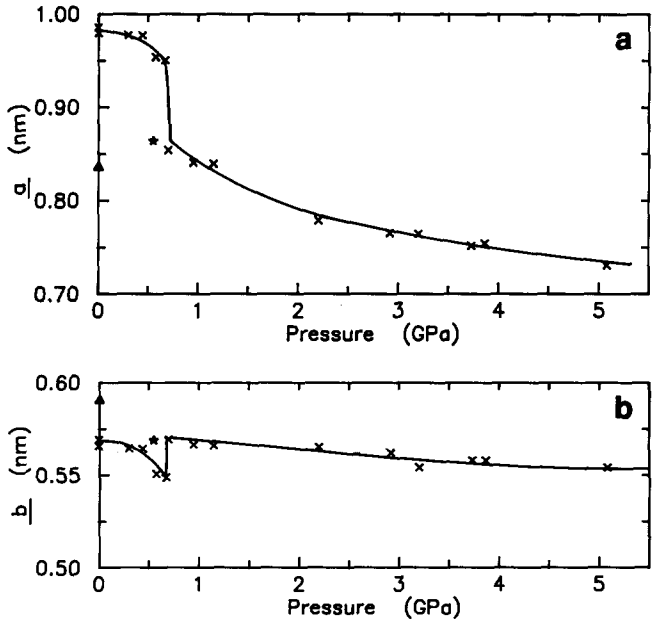

Figure 5 Unit cell dimensions for the orthorhombic structure *versus* pressure. Dimensions in phase II are referred to a centred orthorhombic lattice (see text). Data indicated by filled stars are values from ref. 19 corrected for temperature. Dimensions for the calculated minimum energy structure are shown (Δ). The lines are intended to guide the eye

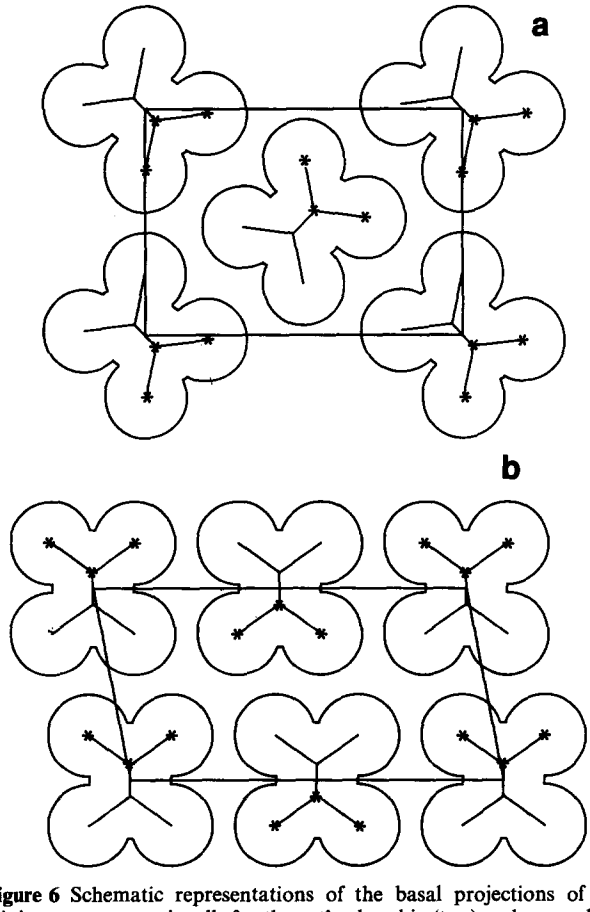

Figure 6 Schematic representations of the basal projections of the minimum energy unit cells for the orthorhombic (top) and monoclinic (bottom) structures. The atoms denoted by an asterisk are in the plane of the paper, while the others are 0.5*c* below the plane

for phase II. This approaches the limit of error. The C–C–C angle exhibits a related change. The ratio of intensities 110/200 did not vary above the pressure at which the transition was complete. The ratio corresponds to a setting angle of 34° which is close to the reported value of 35°[19].

The minimum energy structure determined by empirical pair potential calculations is one that might exist if PTFE were to adopt a stable 2/1 conformation at atmospheric pressure. For the orthorhombic cell in *Figure 6*, the calculated dimensions are $a = 0.837$ nm, $b = 0.591$ nm. As shown in *Figure 5*, the *a* dimension is somewhat smaller than the extrapolation of the experimental data to one atmosphere, while *b* is somewhat larger. The optimum setting angle is 43°, which is significantly larger than the experimental values of 34 and 35°. For a more direct comparison with experiment, the energy of the structure was also minimized with a fixed setting angle of 35°. The dimensions, $a = 0.885$ nm and $b = 0.570$ nm, are in better agreement with the extrapolation of the experimental data. However, the energy is higher by about 0.10 kcal/mol of CF_2. A slightly more favourable comparison of the calculated and experimental values is also obtained if it is made for equal basal areas. In *Figure 7*, the cell parameters and setting angle obtained for energy minimization with a fixed basal area per molecular stem are plotted as a function of the basal area. (The discontinuous nature of the curves results from the size of the increments used in the calculations.) Comparison with *Figure 5* shows that on an equal basal area basis, *a* and *b* are more nearly equal to the experimental values than those resulting from energy minimization with no area constraint.

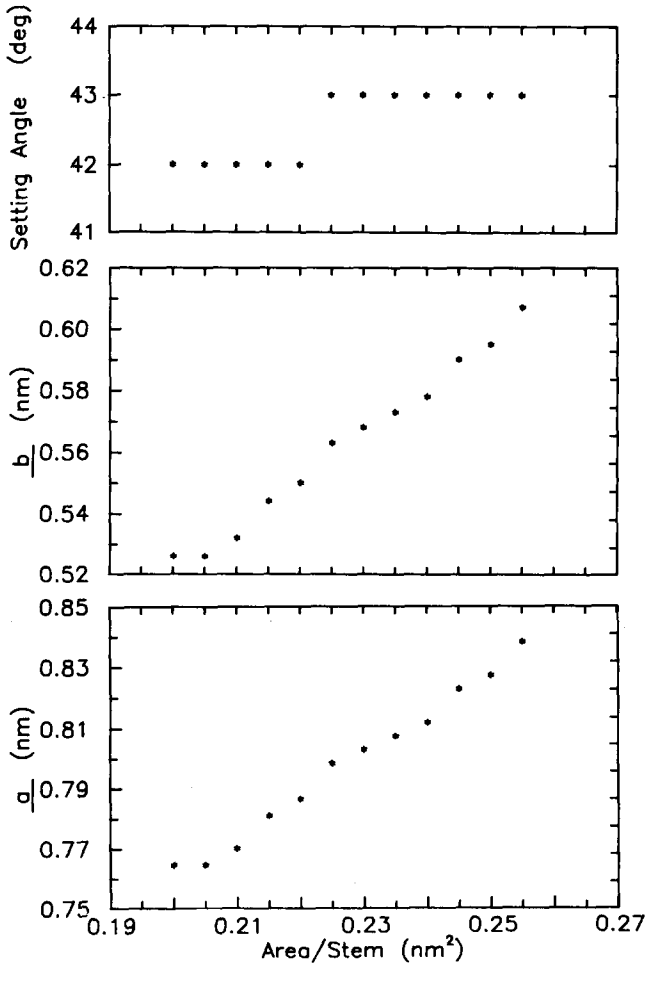

Figure 7 Calculated unit cell dimensions and setting angle for the orthorhombic structure *versus* area per chain stem

Table 1 Values of d^*, the reciprocal of d-spacing, for the monoclinic phase

Pressure (GPa)	Peak #1 (nm^{-1})	Peak #2 (nm^{-1})	Peak #3 (nm^{-1})	Peak #4 (nm^{-1})
2.2	0.209	0.245	0.415	0.462
2.915	0.209	0.246	0.416	0.462
3.73	0.212	0.245	0.423	—
3.865	0.211	0.247	0.422	0.464
5.08	0.216	0.249	0.430	0.466

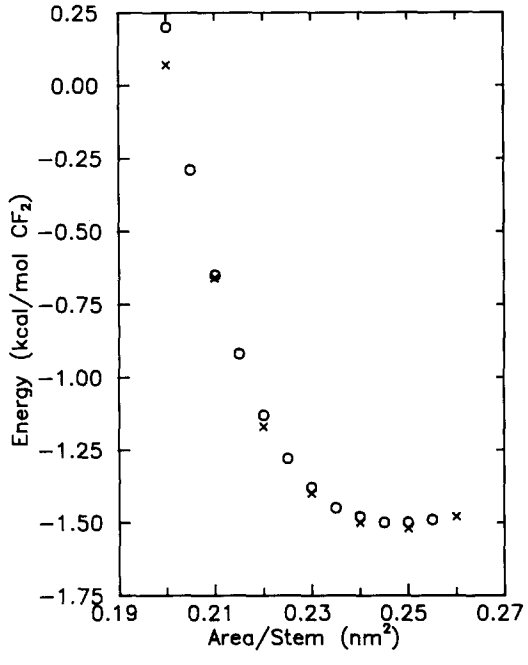

Figure 8 Calculated energies for the orthorhombic (○) and monoclinic (×) structures *versus* area per chain stem

Monoclinic homopolymer

The values of d^* given in *Table 1* for the monoclinic peaks at different pressures can be indexed in several different ways. Several reference points can be used to judge the results. One is the fact that in polyethylene, the orthorhombic and monoclinic unit cell volumes are nearly equal[18]. In view of the similarity of the 2/1 structures for PTFE and polyethylene, it seems plausible to expect a similar result for both. The reported orthorhombic[19] and monoclinic[17] unit cells for PTFE exhibit different volumes, but approximate corrections for the differences in temperature and pressure of the two measurements bring them to nearly the same value.

The volumes of the two structures were also investigated by empirical pair potential calculations. *Figure 8* shows the minimized internal energy as a function of the basal area per molecular stem $(ab \sin \gamma)/2$. The derivative of the energy with respect to the volume at constant temperature is equal to the pressure plus another term which is effectively the same for the two structures. Thus, comparison of the areas and energies for points of equal slope on the two curves amounts to a comparison at equal pressures. The data show that the volume per CF_2 unit is very nearly equal for the two structures.

Finally, it has been demonstrated[18] that the conversion of the orthorhombic, O, cell of polyethylene to the monoclinic, M, takes place by a process that, ideally, would leave M(200) equal to M(010) and O(110), as well as M(210) equal to O(200). Other possible monoclinic cells which fit the orthorhombic lattice but have different relationships among the planes have been discussed[18]. Again, it might be expected that the polyethylene and PTFE behaviour would be similar. In polyethylene, the observed relationships depart from those above because one-half of the molecular stems rotate by about 90° to form the monoclinic structure and this changes the equilibrium packing distances. In PTFE, the basal projection of the molecular stem is more nearly 'square' than that of polyethylene and, therefore, the departures from the relationships above could be expected to be smaller.

For indexing, the three major monoclinic planes with large spacings were assigned in the physically possible combinations to the four peaks observed in the range of d^* from 0.02 to 0.03 nm^{-1}. In some cases, this required that a monoclinic peak be coincident with either another monoclinic or an orthorhombic peak. Since the data did not permit resolution of closely overlapping peaks, this assumption introduced possible error in some peak positions. The peak with a d^* of about 0.046 nm^{-1} was assigned as 111 and that near 0.042 nm^{-1} was assigned as second order of that near 0.021 nm^{-1}. These assignments produced 15 cells which correspond to five different lattices. The basal area per molecular stem ranged from about 0.20 to about 0.24 nm^2 at a pressure near 2 GPa. Since the value for the monoclinic cell is expected to be near that of the orthorhombic (about 0.22 nm^2 near 2 GPa), this range was narrowed to three lattices with area values from 0.21 to 0.23 nm^2. One possible set of indices for each is shown in *Table 2*. (There are others which yield the same areas.) These represent various approximations to the possible relationships proposed for the orthorhombic and monoclinic polyethylene cells[18]. In the present samples, the stresses other than hydrostatic result from the elastic inhomogeneities. Thus, the stress is not so well known and probably not the same as that in reference 18. As a result, the conversion route could be different from that demonstrated for one stress state in polyethylene[18].

The number of cases in *Table 2* cannot be reduced further with certainty. Case 3 might be taken as the correct unit cell since it yields the basal area most nearly equal to that observed experimentally for the orthorhombic structure. This is shown by the plot of basal area per molecular stem for the two structures as a function of pressure in *Figure 9*. The corrected basal area per stem for the orthorhombic cell from reference 19 is also shown. It represents a reasonable extrapolation of the present data. The data for case 3 closely match the orthorhombic data, but the data for cases 2 and 1 do not match as well. The basal area per stem for the monoclinic cell from reference 17 is also shown. It has been corrected from the measurement temperature of

Table 2 Selected assignments of the monoclinic indices

Peak	Case 1	Case 2	Case 3
M1	$1\bar{1}0$	$1\bar{1}0$	010
M2	110	200	$2\bar{1}0$ 200
M3	$2\bar{2}0$	$2\bar{2}0$	020
M4	111	111	111
OR110	M200	–	–
OR200	–	M110	–

21°C (ref. 17) to 27°C. If the present experimental data for the monoclinic cell extrapolate parallel to the orthorhombic, the area from reference 17 represents a reasonable extrapolation of the present data. Energy calculations were also made for the minimum energy monoclinic structure at atmospheric pressure. For the monoclinic cell in *Figure 6*, the calculated parameters are $a = 0.984$ nm, $b = 0.513$ nm and $\gamma = 101°$. As shown in *Figure 9*, it represents a reasonable extrapolation of the experimental data. The same is true for the calculated orthorhombic cell which superposes in *Figure 9*.

While case 3 is favoured by comparison of the basal area with that of the orthorhombic, comparison of its cell parameters with the earlier[17] experimental ones is not so favourable. This is shown in *Table 3* with the earlier data (corrected to 27°C) given for 1.2 GPa and the present for 2.2 GPa. The value of a for case 3 is smaller than the earlier one, but could plausibly increase to that value with decreasing pressure. Also, the two values of γ are in reasonable agreement. However, b presents a question since the present value is larger. It is not likely that this higher pressure value would decrease with decreasing pressure.

Consideration of alternate unit cells which fit the two lattices does not resolve the question. The cell parameters for cases 1 and 2 are also given in *Table 3*. Both are in more plausible agreement with the earlier experimental data. The results of energy minimization calculations, with the basal area fixed to match the four sets discussed above, are also given. The calculated results are in best agreement with the case 1 and the earlier[17] results. Thus, case 1 might be taken as correct since it yields the most plausible agreement of unit cell parameters with both the earlier experimental results and the results of energy calculations. However, as noted above, the basal area for case 1 (and 2) is not in close agreement with that of the orthorhombic. Further, the earlier experimental results might be influenced by the presence of residual amounts of the orthorhombic structure and the stress state is probably different from that for the present measurements. The question cannot be resolved at present. Cases 1 and 3 represent the more likely unit cells.

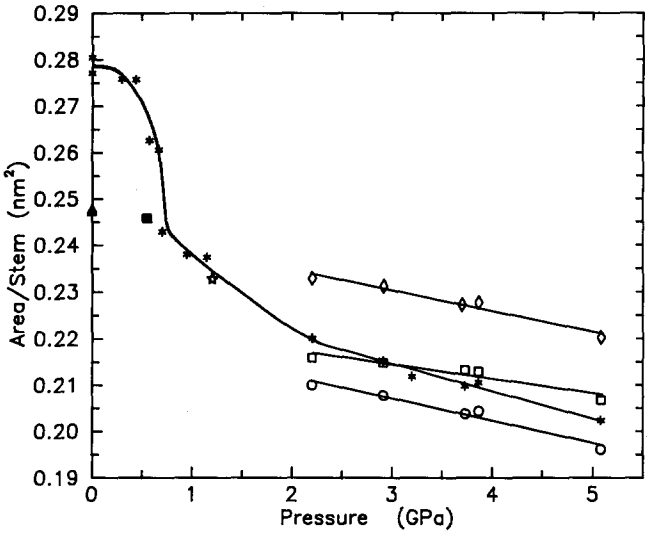

Figure 9 Basal area per chain stem *versus* pressure. *, Data for the orthorhombic structure; ■, ☆, data from ref. 19 and 17 respectively; Δ, results from energy calculations superimpose. ◇, ○, □, Monoclinic cases 1, 2 and 3 from *Table 2* respectively. The line at low pressures for the orthorhombic structure is intended to guide the eye. The lines drawn through the data between 2 and 5 GPa represent least-squares fits to the data

Conformation and orientation disorders

The excess energies of the defects are presented with respect to the energy of the perfect crystal. Therefore, *Table 4* shows the internal energies of the molecule in the monoclinic and orthorhombic structures. The energies which were calculated with the same model for the low pressure phases are included for comparison[12]. The difference between the total energy of phase II and the orthorhombic structure in III is of the same order but larger than the value calculated for one atmosphere from experimental data[29] and the value obtained by integrating the appropriate functions constructed from experimental PVT curves[30]. The agreement is improved if the calculation in reference 29 is repeated with the PVT data presented in reference 30. The total energy of the monoclinic structure is slightly lower than that of the orthorhombic and, for the calculated unit cells discussed above, the basal area of the monoclinic cell is slightly greater than that of the orthorhombic. These results differ a little from those for polyethylene in which both the area and energy of the monoclinic are smaller than those of the orthorhombic[31]. To the extent that the present rather small differences are accurate and that the entropies of the monoclinic and orthorhombic phases are equal, various relative transition pressures can be calculated. Using the total internal energies in *Table 4* together with volumes given here and previously[12], leads to the result that the orthorhombic structure is the thermodynamically favoured one for the pressures at which the helical structures of phases I and II would transform to the 2/1 structures. Thus, the thermodynamic results are consistent with the necessity for shear stress in the formation of the monoclinic structure. Other parameters that could influence the result are the molecular mechanism and the kinetics of the transition to phase III[15].

Consideration of the entropies is, of course, also

Table 3 Selected monoclinic unit cells

Parameter	Ref. 17[a]	Calc.[b]	Case 3[c]	Calc.[b]	Case 2[c]	Calc.[b]	Case 1[c]	Calc.[b]
a (nm)	0.957	0.956	0.904	0.926	0.852	0.920	0.944	0.954
b (nm)	0.505	0.498	0.529	0.477	0.508	0.470	0.503	0.497
γ (°)	105.5	101.8	115.3	102.2	104.0	103.8	102.5	101.9
Basal area/molecular stem (nm²)	0.233	0.233	0.216	0.216	0.210	0.210	0.232	0.232

[a] 1.2 GPa
[b] Calculated for the same basal area as the experimental case in the preceding column
[c] 2.2 GPa

Table 4 Conformational, packing, and total internal energies of the molecule

Phase	I[a]	II[a]	III	III
Conformation	15/7	54/25	2/1	2/1
Structure	Hexagonal	Triclinic	Orthorhombic	Monoclinic
Non-bonded conformational energy [kcal/mol CF_2]	3.29	3.37	3.08[a]	3.08[a]
Bonded conformational energy [kcal/mol CF_2]	7.70	7.41	9.60[a]	9.60[a]
Total conformational energy [kcal/mol CF_2]	10.99	10.78	12.68	12.68
Packing energy [kcal/mol CF_2]	−2.39	−2.38	−2.93	−2.94
Total energy [kcal/mol CF_2]	8.60	8.40	9.75	9.74

[a]From reference 12

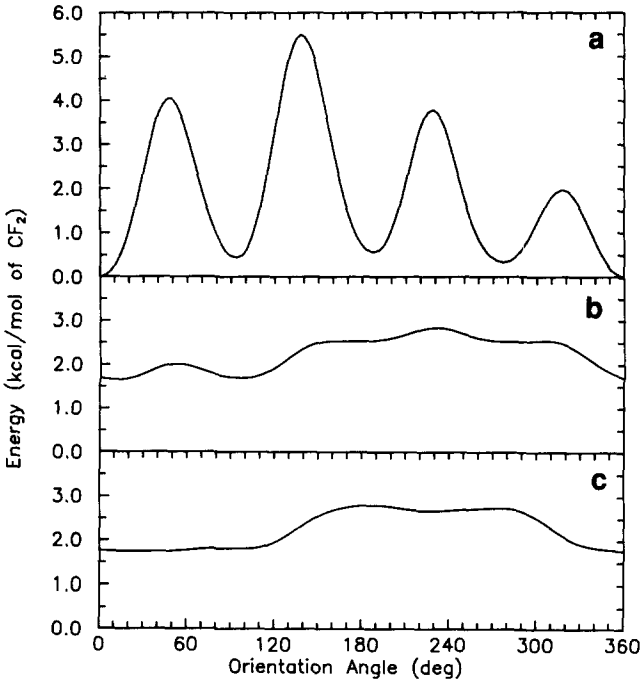

Figure 10 Calculated energies *versus* orientation angle for defect molecular stems placed at the position of the central molecule of the nine-stem orthorhombic array depicted in *Figure 1*. The orientation angle is measured with respect to the crystallographic (minimum energy) setting angle. Rotation (a) of a 2/1 stem; (b) rotation of a 54/25 stem; (c) rotation of a 15/7 stem

necessary. Application of the Clayperon equation shows $\Delta S_{II,I}$ and $\Delta S_{II,III}$ to be positive with $\Delta S_{I,III}$ negative. One aspect of the entropies which can be addressed by modelling calculations is that introduced by conformational and rotational defects[12]. *Figure 10* shows the energies *versus* rotational orientation for 2/1, 15/7 and 54/25 molecular segments placed in the centre of the nine-stem model having the perfect orthorhombic structure. The corresponding data for the monoclinic structure are very similar.

In view of the nearly square cross-section of the PTFE molecule in the 2/1 conformation, it is not too surprising that the energy differences between crystallographic orientations and those 90° greater are small for the 2/1 rotational defect in both the orthorhombic and monoclinic structures. A helical defect, while being of higher energy than the minima of the 2/1 defect, is fairly uniform in energy with orientation. The low-energy defects for each conformation were minimized by the method discussed above. The results given in *Table 5* are generally similar for both structures. Those associated with the 2/1 conformation are of the order of a few tenths of a kcal/mol CF_2. For either 15/7 or 54/25 helical segments, the energies are of the order of one kcal/mol CF_2 as a result of the larger volume required to accommodate the helix. The increase in the area/stem is about three times that required for the 2/1 rotational defect. The helical defects in the high pressure phases also exhibit a higher energy and cause more increase in the area/stem than comparable conformational defects in phases I and II[12].

The total internal energy of such defects includes not only the intermolecular terms in *Table 5* but also the intramolecular energies in *Table 4*. Intramolecular interfacial energies[12] between segments of the same molecule in different conformations and/or rotations can be neglected if the defect sequences are long enough or if the interfacial energies are similar. Then the 54/25 and 15/7 defects become reasonably low energy ones because their conformational energies are lower than that for the 2/1 conformation. Of course, the numbers in *Table 5* are for atmospheric pressure and increasing the pressure would reduce the basal area, thereby increasing the energies for all the defects. With increasing pressure, there would be another energy contribution equal to $P\Delta V$, with ΔV being a consequence of the extra basal area resulting from the defect. The latter energy would not be too large even at 5 GPa and, to a first approximation, the former would be similar for all the defects. Therefore, the results suggest that the 54/25 and 15/7 defects could exist along with the 2/1 rotational defects.

Consideration of the small variation of the energy with setting angle (*Figure 10*) suggests that the many possible orientational states of the helical defects could make phase III a higher entropy phase than II for which the variation of energy with orientation is greater[12]. The reduced force constants for torsional oscillations of the 2/1 chain would also contribute to the higher entropy of phase III[29]. Both effects agree qualitatively with the result obtained with the Clapeyron equation. Both also agree qualitatively with fluorine n.m.r. data[32]. Narrowing of the fluorine resonance at the transition from phase II to III has been interpreted as resulting from molecular rotation. The flat curve in *Figure 10* suggests the likelihood of not only many orientational states but also molecular rotation by various mechanisms. The latter could involve diffusion along the molecule of points at which the setting angle of the helix changes.

The entropy difference between phases III and I is not clear when considered qualitatively. The Clapeyron equation together with the phase diagram and the volumes of transition indicate that the difference between the entropies of phases I and III should be smaller than that between II and III, with phase I having the highest

Table 5 Relaxed intermolecular defect energies in phase III

Structure	Conformation of defect molecule	Excess energy [kcal/mol CF_2]	Change of *a* (nm)	Change of *b* (nm)	Change of area/stem (nm^2)	*c* shift (nm)	Setting angle[c] (deg)
Orthorhombic	2/1	0.24	−0.003	0.005	0.0012	0.000	83
Orthorhombic	15/7[a]	1.08	0.010	0.001	0.0033	0.007	99
Orthorhombic	54/25[a]	1.06	0.009	0.002	0.0035	0.000	96
Monoclinic	2/1	0.20	0.008	0.002	0.0001[b]	0.000	92
Monoclinic	15/7[a]	1.13	0.010	0.006	0.0025[b]	0.007	116
Monoclinic	54/25[a]	1.13	0.012	0.006	0.0030[b]	0.007	99

[a]This result is for a right-handed defect molecule. The result for the left-handed molecule is very similar and is not given here
[b]The angle, γ, changed from 101 to 104°. For the other cases, it did not change
[c]Relative to the perfect crystal value

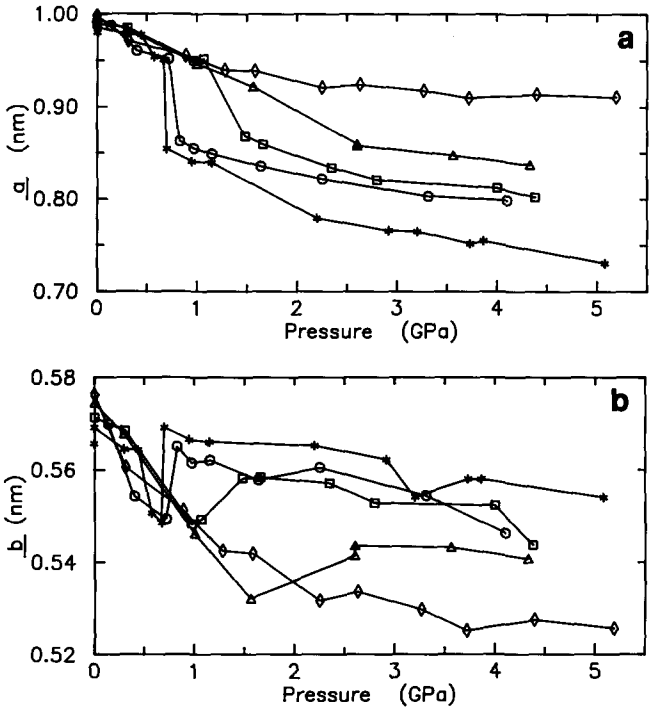

Figure 11 Unit cell dimensions for the series of copolymers *versus* pressure. For defect concentrations expressed as CF_3/CF_2 the symbols correspond as follows: *, 0.0; ○, 0.008; □, 0.018; △, 0.038; ◇, 0.049

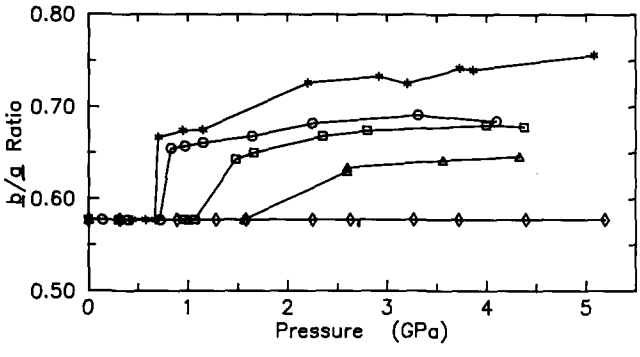

Figure 12 Ratio of *b*/*a* cell dimensions for the series of copolymers *versus* pressure. The symbols are the same as in *Figure 11*

entropy. This seems possible since the defect energies for phase I are smaller than those for phase II[12]. Further, there are many possible crystal structures with low energies[12]. Both effects would make the entropy of phase I greater than that of phase II and, therefore, possibly greater than that of phase III.

Perfluoromethyl disorders

The powder patterns at 27°C for the copolymers correspond to phase I as a result of the II–IV and IV–I transition temperatures being lowered by the CF_3 units[6]. The patterns of phase I are less complex than those of phase II, and those of the copolymers are more diffuse than those of the homopolymer[13]. There is no evidence of the monoclinic structure. This probably results because the copolymer can flow in the melt and therefore does not have pores resulting from sintering. Further, crystals of the copolymer are much smaller than those of the homopolymer. Both effects reduce the elastic inhomogeneities which lead to the shear stress required to form the monoclinic phase.

The unit cell dimensions, *a* and *b*, are plotted as a function of pressure in *Figure 11*. The transition from phase I (II for the homopolymer) to phase III shifts to higher pressure with increasing CF_3 concentration. This is more readily evident in the ratio *b*/*a* which is plotted as a function of pressure in *Figure 12*. The ratio 0.577 corresponds to the hexagonal structure and higher values to the orthorhombic. With increasing CF_3 concentration, the departure of the orthorhombic structure from the hexagonal ratio becomes smaller because the CF_3 units cause a substantial increase of the orthorhombic *a* and a small decrease of *b*. (In ethylene–propylene copolymers, both increase[33].) This shifts the packing of the 2/1 molecules toward metrically hexagonal. Molecular modelling indicates that to accommodate the CF_3 unit, the conformation of the molecule must be distorted near the position of the unit. On opposite sides of the CF_3, the orientation of the plane of the backbone can be the same or different by 90° (*Figure 13*) with approximately equal excess intramolecular energy. These orientations correspond to two of the minima in *Figure 10a*. In both cases, the distortion would help shift the structure toward metrically hexagonal. In contrast, the increase of cell dimension with CF_3 concentration clearly is much smaller in the low pressure phase as has been demonstrated more precisely with powder diffractometer data[34]. As a consequence of this difference between the phases, the volume of transition shown in *Figure 14* decreases with increasing CF_3 concentration and extrapolates to zero at 0.049 CF_3/CF_2. In the present measurements, a transition cannot be identified with certainty up to 5.19 GPa for the sample with 0.049 CF_3/CF_2. The slope of the line corresponds to a CF_3 (defect) transition volume of 4.2×10^{-2} nm^3/CF_3. The transition volume

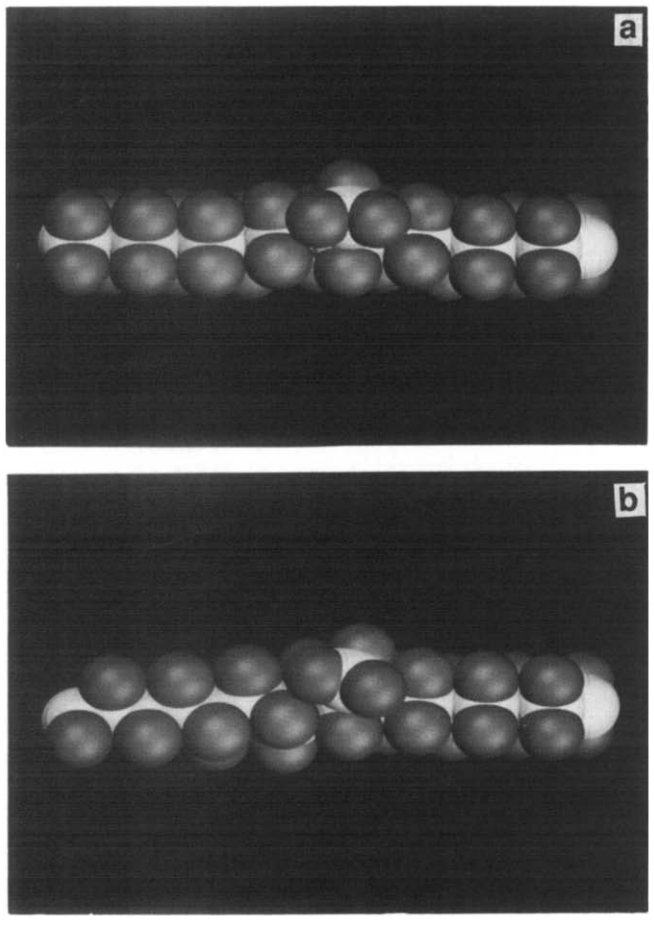

Figure 13 The results of molecular modelling showing the defect structure associated with a perfluoromethyl group. Conformations having no change (a) away from the CF_3 unit or a 90° rotation (b) of the orientation of the plane of the backbone have nearly equal intramolecular energies

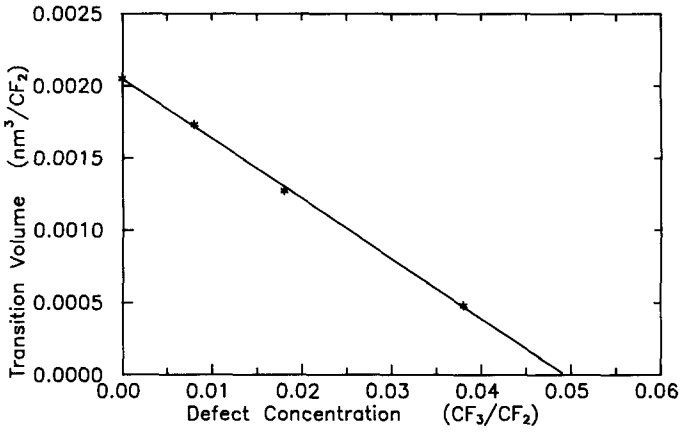

Figure 14 Volume of transition *versus* CF_3 concentration. The line is a least-squares fit to the data

for the homopolymer, -2.1×10^{-3} nm^3/CF_2, is in the range of reported values[1,30]. Any variation of c with CF_3 concentration in both phases is within the present limit of error.

The crystal compressibility of the orthorhombic structure above 2 GPa is 0.029 GPa^{-1} for the homopolymer and appears to decrease about 0.34 GPa^{-1}/(CF_3/CF_2). The result for the homopolymer is comparable to the bulk compressibility of 0.072 GPa^{-1} which was determined experimentally[1,30] and includes the substantial contributions of the amorphous material. The average crystal compressibility of the case 1 and 3 homopolymer monoclinic structures discussed above is 0.017 GPa^{-1}. For the hexagonal structure at high pressure (the sample with 0.049 CF_3/CF_2), the compressibility is 0.01 GPa^{-1}. Below the transition pressure, the crystal compressibility of this structure is approximately 0.092 GPa^{-1} for all CF_3 concentrations. This is comparable to the bulk compressibility of 0.12 GPa^{-1} which also includes the contributions of the amorphous material[30].

Phase diagram

The reciprocal pressure *versus* CF_3 concentration phase diagram in *Figure 15* shows points and lines based on either the present or earlier[6,33] experimental data. The line for phase II is not based on data and is indicated for clarity only. It is known on the basis of the present data, however, that the sample with 0.008 CF_3/CF_2 exhibits only the phase I structure. Thus, the dashed I–II boundary must intersect the I–III boundary at a concentration less than 0.008. The lower pressure limit of the transition to phase III is taken as the lowest pressure at which the hexagonal 100 peak can be perceived as beginning to split into the orthorhombic 110/200 pair. The upper limit is taken as the pressure above which the ratio of intensities 110/200 can no longer be perceived to decrease. The average of these two is taken as the transition pressure. There are some uncertainties because data were not always obtained just above and below the pressure of interest.

Between the limits above, there is a range of pressure in which both the hexagonal 100 and the orthorhombic 110,200 appear to be present. This has been observed for the homopolymer and attributed to fluctuations in structure[15]. In the present case it might be associated with distributions in CF_3 concentration, molar mass, and lamella thickness as well as fluctuations in structure. All would spread the transition over a range of pressures.The transition is rather wide at high CF_3 concentration but decreases markedly with decreasing concentration. The kinetic effects reported for the II–III transition[15] could also contribute to the apparent width of the transition. However, this seems unlikely for the present data in view of both the higher temperature of measurement and the longer time required for each of the measurements. At

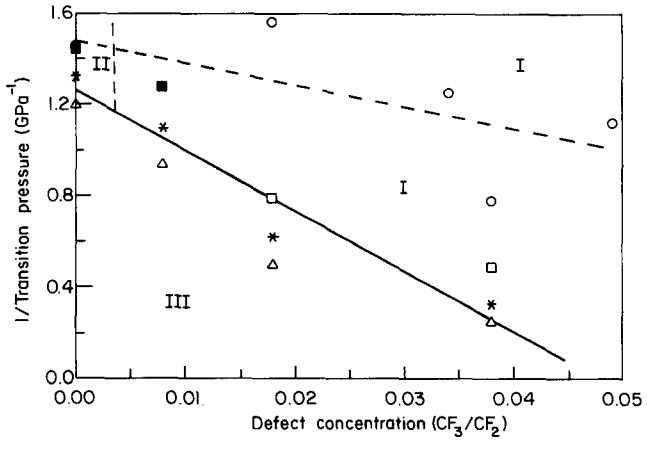

Figure 15 Reciprocal pressure *versus* CF_3 concentration. *, transition pressures; Δ, □, respectively, the upper and lower limits of the pressures over which the transition occurs. ○, The pressures at which the molecules adopt, on average, a 2/1 conformation. Filled symbols denote overlapping squares and circles

pressures below those at which the 110,200 split appeared, the 107 and 108 peaks of the hexagonal structure merged to indicate a space–time average 2/1 conformation of the molecule. Thus, the structure becomes metrically hexagonal. This starts at about 0.69 GPa for the homopolymer and appears to increase slightly with CF_3 concentration (broken line). The effect has been observed in the homopolymer and attributed to thermal oscillation of the molecules between left- and right-handed conformations as well as irregular untwisting[15,35].

For a very dilute solution of one non-interacting species in another, the molar Gibbs free energy, G, of the solution can be approximated as[36]:

$$G = (1 - X)\mu_0 + X\mu_d \quad (1)$$

In the present case, μ_0 is the chemical potential of the pure homopolymer and μ_d is the chemical potential of the solute (the CF_3 defects). X is the mole fraction of solute. Using Δ for the changes across the phase boundary, equation (1) can be shown to yield

$$P = P_0 - (\Delta\bar{U}_d + P\Delta\bar{V}_d - T\Delta\bar{S}_d)X/\Delta V_0 \quad (2)$$

Here, P is the transition pressure. P_0 and ΔV_0 are the transition pressure and the molar transition volume of the homopolymer, respectively. $\Delta\bar{U}_d$, $\Delta\bar{V}_d$ and $\Delta\bar{S}_d$ are the partial molal internal energy, volume and entropy of transition of the defect, respectively. Since the mole fraction of CF_3 defects would be expected to be the same in both phases, $\Delta\bar{S}_d$ can be taken as zero. Using the number given above for $\Delta\bar{V}_d$, yields values for $P\Delta\bar{V}_d$ of about 6 and 30 kcal/mol CF_3 for pressures of 1 and 5 GPa, respectively. In phase I, $\bar{U}_d$ is about 1 kcal/mol CF_3[37]. Since the energy of such defects is proportional to the modulus of the host material[38] and since the modulus of phase III is less than twice that of I[30,39], $\Delta\bar{U}_d$ should be less than 1 kcal/mol CF_3. Therefore, equation (2) can be approximated as

$$1/P = 1/P_0(1 + \Delta\bar{V}_d X/\Delta V_0) \quad (3)$$

In *Figure 15*, the few data for the transition fit a straight line. Further, the slope and intercept produce a value of -21.5 CF_2/CF_3 for $\Delta\bar{V}_d/\Delta V_0$ in reasonable agreement with the value of -20 CF_2/CF_3 based on the numbers given above for $\Delta\bar{V}_d$ and ΔV_0. Thus, it can be concluded that the fact that the CF_3 units enlarge the cell of phase III much more than phase I is the primary reason for the increase of transition pressure with CF_3 concentration.

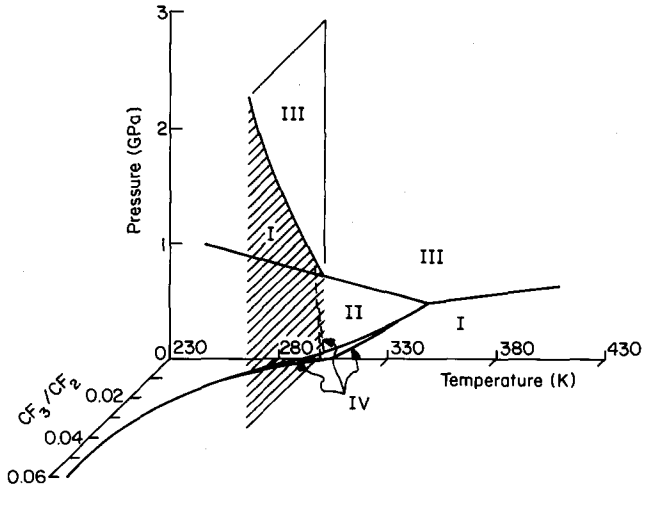

Figure 16 The pressure, temperature, CF_3 concentration phase diagram. The locations of solid lines have been experimentally established, while those of the broken lines have not

As pointed out above, phase I is metrically hexagonal at pressures above the one at which the molecules adopt a space–time average 2/1 conformation. It was also observed that phase III approaches a metrically hexagonal structure as the CF_3 concentration is increased. The variation of the b/a ratio with CF_3 concentration indicates that it becomes so at a CF_3 concentration a little over 0.05 CF_3/CF_2. This is also the approximate concentration at which the specific volume of the two phases becomes equal (*Figure 14*). Thus, the conformation, packing and specific volume of the two phases approach one another at 27°C as the CF_3 concentration approaches 0.05 CF_3/CF_2 and the pressure exceeds 3.5 GPa. A transition cannot be observed at pressures to 5 GPa in a sample with a CF_3 concentration of 0.049 CF_3/CF_2. These are the characteristics of a critical point. It is possible that the simplifying assumptions made earlier are incorrect and that the transition still occurs at a higher pressure. However, it seems likely that the differences of entropy, internal energy, etc. between two such similar structures are also zero and a true critical point exists. Thermal and light scattering measurements would help to confirm the fact.

The pressure, temperature, CF_3 concentration phase diagram is shown in *Figure 16*. It is evident that thermal measurements over a range of p, T and X would provide useful additional information.

CONCLUSION

The monoclinic structure of PTFE can be formed in phase III even when the sample is subject to hydrostatic pressure. It is likely that elastic inhomogeneities in the sample lead to shear stresses which produce the monoclinic structure. Energy calculations for the monoclinic and orthorhombic structures are consistent with this possibility. These calculations also indicate that conformational and rotational disorders raise the entropy of phase III. Perfluoromethyl comonomer units cause the I–III transition pressure to increase with increasing CF_3 concentration. This occurs primarily because the CF_3 groups enlarge the unit cell in phase III much more than in phase I. With increasing pressure, the structure of phase I becomes metrically hexagonal and the structure of phase III does the same at a CF_3 concentration of about 0.05 CF_3/CF_2. Both exhibit a 2/1 molecular conformation. Further, the volume of transition becomes zero at the same concentration and a transition cannot be observed to a pressure of 5.2 GPa in a sample with a concentration of 0.049 CF_3/CF_2. Thus, there appears to be a critical point at 27°C for a CF_3 concentration near 0.05 CF_3/CF_2 and a pressure between 3.5 GPa and 5.2 GPa.

ACKNOWLEDGEMENTS

Portions of the work of R.K.E., E.S.C. and B.L.F. were carried out in the National Institute of Standards and Technology, Gaithersburg, MD 20899, USA.

REFERENCES

1 Weir, C. E. *J. Res. Nat. Bur. Stand.* 1953, **50**, 95; Bridgman, P. W. *Proc. Amer. Acad.* 1948, **76**, 71
2 Rigby, H. A. and Bunn, C. W. *Nature* 1949, **164**, 583
3 Beecroft, R. I. and Swenson, C. A. *J. Appl. Phys.* 1959, **30**, 1793
4 Quinn Jr, F. A., Roberts, D. E. and Work, R. N. *J. Appl. Phys.* 1951, **22**, 1085
5 Martin, G. M. and Eby, R. K. *J. Res. Nat. Bur. Stand.* 1968, **72A**, 467
6 Weeks, J. J., Sanchez, I. C., Eby, R. K. and Poser, C. I. *Polymer* 1980, **21**, 325
7 Bunn, C. W. and Howells, E. R. *Nature* 1954, **174**, 549
8 Clark, E. S. and Muus, L. T. *Z. Krist.* 1962, **117**, 119
9 Clark, E. S. and Muus, L. T. *Z. Krist.* 1962, **117**, 109
10 Weeks, J. J., Clark, E. S. and Eby, R. K. *Polymer* 1981, **22**, 1480
11 Farmer, B. L. and Eby, R. K. *Polymer* 1981, **22**, 1487
12 Farmer, B. L. and Eby, R. K. *Polymer* 1985, **26**, 1944
13 Weeks, J. J., Clark, E. S. and Eby, R. K. *Polymer* 1981, **22**, 1496
14 Brown, R. G. *J. Chem. Phys.* 1964, **40**, 2900
15 Matsushige, K., Enoshita, R., Ide, T., Yamauchi, N., Taki, S. and Takemura, T. *J. Appl. Phys.* (*Japan*) 1977, **16**, 681; Nicol, M. F., Wiget, J. M. and Wu, C. K. *J. Polym. Sci., Polym. Phys. Edn.* 1980, **18**, 1087
16 Dzhavadov, L. N. and Krotov, Yu. I. *Inzh. Fiz. Zh.* 1980, **39**, 671; Tanaka, H. and Takemura, T. *Polym. J.* 1980, **12**, 355
17 Flack, H. D. *J. Polym. Sci.* 1972, **A-2 10**, 1799
18 Seto, T., Hara, T. and Tanaka, K. *J. Appl. Phys.* (*Japan*) 1968, **7**, 31
19 Nakafuku, C. and Takemura, T. *J. Appl. Phys.* (*Japan*) 1975, **5**, 599
20 Kavesh, S. and Schultz, J. M. *J. Polym. Sci.* 1970, **A-2 8**, 243
21 Munro, R. G., Block, S., Piermarini, G. J. and Mauer, F. A. in 'Materials Science Research' (Eds R. F. Davis, H. Palmour and R. L. Porter), 1984, **17**, 783
22 Piermarini, G. J., Block, S. and Barnett, J. D. *J. Appl. Phys.* 1973, **44**, 5377
23 Barnett, J. D., Block, S. and Piermarini, G. J. *Rev. Sci. Instrum.* 1973, **44**, 1
24 Boone, M. B. and Clark, E. S. *Bull. Am. Phys. Soc.* 1985, **30**, 488; Boone, M. B., MS Dissertation, University of Tennessee, Knoxville, 1984
25 Bunn, C. W., Cobbold, A. J. and Palmer, R. P. *J. Polym. Sci.* 1958, **28**, 365; Melillo, L. and Wunderlich, B. *Kolloid-Z. u. Z. Polymere* 1972, **250**, 417; Bassett, D. C. and Davitt, R. *Polymer* 1974, **15**, 721
26 Nemat-Nasser, S. and Horii, H. *J. Geophys. Res.* 1982, **87**, 6805
27 Horii, H. and Nemat-Nasser, S. *J. Geophys. Res.* 1985, **90**, 3105
28 Eshelby, J. D. *J. Appl. Phys.* 1954, **25**, 255
29 Bates, T. W. and Stockmayer, W. H. *Macromolecules* 1968, **1**, 17
30 Weir, C. E. *J. Res. Nat. Bur. Stand.* 1954, **53**, 245; Lupton, J. M. *SPE Trans.* 1961, **1**, 105
31 Farmer, B. L. and Eby, R. K. *Polymer* 1979, **20**, 363
32 Nakafuku, C., Taki, S. and Takemura, T. *Polymer* 1973, **14**, 558
33 Sella, C. *Compt. Rend.* 1959, **248**, 2348; Walter, E. R. and Reding, F. P. *J. Polym. Sci.* 1956, **21**, 561
34 Bolz, L. H. and Eby, R. K. *J. Res. Nat. Bur. Stand.* 1965, **69A**, 481
35 Muus, L. T. and Clark, E. S. *Polym. Prepr.* 1964, **5** (1), 17
36 Landau, L. E. and Lifschitz, E. M. 'Statistical Physics' Chapter IX, Oxford University Press, Oxford, 1938
37 Sanchez, I. C. and Eby, R. K. *J. Res. Nat. Bur. Stand.* 1973, **77A**, 353
38 Eshelby, J. D. *Solid State Phys.* 1956, **3**, 79
39 Matsushige, K., Hirakawa, S. and Takemura, T. *Mem. Faculty of Eng. Kyushu Univ.* 1972, **32** (2), 153